




RESEARCH ARTICLE OPEN ACCESS

Effect of Ga Variation on the Bulk and Grain-Boundary Properties of Cu(In,Ga)Se₂ Absorbers in Thin-Film Solar Cells and Their Impacts on Open-Circuit Voltage Losses

Sinju Thomas¹ | Wolfram Witte²  | Dimitrios Hariskos²  | Stefan Paetel²  | Chang-Yun Song³ | Heiko Kempa³  | Matthias Maiberg³ | Nora El-Ganainy⁴ | Daniel Abou-Ras¹ 

¹Department Structure and Dynamics of Energy Materials, Helmholtz-Zentrum Berlin für Materialien und Energie GmbH, Berlin, Germany | ²Zentrum für Sonnenenergie- und Wasserstoff-Forschung Baden-Württemberg (ZSW), Stuttgart, Germany | ³Martin-Luther-Universität Halle-Wittenberg, Institut für Physik, Fachgruppe Photovoltaik, Halle (Saale), Germany | ⁴Competence Centre Photovoltaics Berlin (PVcomB)/Helmholtz Zentrum Berlin für Materialien und Energie (HZB), Berlin, Germany

Correspondence: Daniel Abou-Ras (daniel.abou-ras@helmholtz-berlin.de)

Received: 26 May 2023 | **Revised:** 22 May 2024 | **Accepted:** 21 August 2024

Funding: This work was supported by Bundesministerium für Wirtschaft und Klimaschutz: BMWK [03EE1059B (HZB); 03EE1059A (ZSW); 03EE1059C (MLU)].

Keywords: Cu(In,Ga)Se₂ absorbers | electron lifetime | Ga variation | grain boundaries | open-circuit voltage losses | thin-film solar cells

ABSTRACT

Polycrystalline widegap Cu(In,Ga)Se₂ (CIGSe) absorbers for top cells in photovoltaic tandem devices can be synthesized via [Ga]/([Ga] + [In]) (GGI) ratios of > 0.5. However, the power conversion efficiencies of such high-GGI devices are smaller than those of the record cells with GGI < 0.5. In the present work, the effects of the GGI ratio on various CIGSe material properties were studied and correlated with the radiative and nonradiative open-circuit voltage (V_{OC}) deficits of the thin-film solar cells. Average grain sizes, grain boundary (GB) recombination velocities, fluctuations in luminescence energy distribution, barrier heights at GBs, effective electron lifetimes, and Urbach energies were investigated in five solar cells with GGI ratios from 0.13 to 0.83. It was found that the GGI variation affects GB recombination velocities, fluctuations in spatial luminescence distributions, the average grain size, the electron lifetime, and the Urbach energy. In contrast, the detected ranges of barrier heights at GBs are independent of the GGI ratio. Mainly Ga/In gradients give rise to substantial radiative V_{OC} losses in all solar cells. Nonradiative V_{OC} deficits are dominant especially for solar cells with GGI > 0.5, which can be attributed to low bulk lifetimes and enhanced recombination at GBs in CIGSe absorbers in this compositional range.

1 | Introduction

Polycrystalline thin-film solar cells based on Cu(In,Ga)Se₂ (CIGSe) absorber layers exhibit record power conversion efficiencies of up to 23.4% in case the integral [Ga]/([Ga] + [In]) (GGI) ratio in the CIGSe absorber is about 0.3 [1]. The band-gap energy E_g of a CIGSe thin film can be adjusted via its integral GGI ratio as E_g varies between about 1.04 [2] and 1.68 eV [3] for GGI ratios of between 0 (CuInSe₂) and 1 (CuGaSe₂). While devices with low-gap CIGSe absorber layers have already exhibited

high power conversion efficiencies [4], solar-cell devices with widegap CIGSe layers (GGI > 0.5) that can be used, for example, as absorber layers for top cells in tandem devices [5], generally feature efficiencies much smaller than those at the theoretical, radiative (Shockley–Queisser) limit [6, 7], mainly owing to very large losses in the open-circuit voltage (V_{OC}).

Numerous reports in the literature gave possible reasons for the deterioration of the solar cell performance when the GGI ratio becomes larger than about 0.4–0.5. Increasing GGI decreases

This is an open access article under the terms of the [Creative Commons Attribution](https://creativecommons.org/licenses/by/4.0/) License, which permits use, distribution and reproduction in any medium, provided the original work is properly cited.

© 2024 The Author(s). Progress in Photovoltaics: Research and Applications published by John Wiley & Sons Ltd.

the lattice parameters c and a thereby $c/a < 2$. An ideal tetragonal crystal structure with minimum defect density occurs at $c/a = 2$ at a GGI around 0.2 [8]. This change in the crystal structure due to GGI increase results in lattice strain that is linked to the density of extended defects. The Cu antisite-defect concentration increases with GGI [9]. According to Spindler et al. [10], at GGI values of about 0.5 and for $E_g > 1.35$ eV, the energy states of donor-type defects are extended into the band-gap region, thus, they are deep defects. Therefore, the alteration in the states occupied by these defects and increased defect concentration at $GGI > 0.5$ enhances the probability of defect-assisted recombination, resulting in a higher V_{OC} deficit (ΔV_{OC}). Charge-carrier recombination at the heterointerface between CIGSe and the buffer layer due to an unfavorable conduction-band offset also may contribute to losses in V_{OC} [11, 12]. Furthermore, also increasing point-defect concentration and trap densities as well as smaller minority-charge carrier diffusion lengths are reported as consequences of an increase in GGI [9, 13–15].

Although GGI variations in CIGSe thin films for solar cells have been performed and analyzed intensively in the past, some aspects such as the grain-boundary (GB) recombination behavior, the barrier heights at the GBs, electron recombination velocity at the GBs and the distribution of the luminescence energy with respect to the GGI ratio have not yet been analyzed in detail. More generally, it would be desirable to assess microscopic structure–property relationships in CIGSe layers, linking microstructural with optoelectronic absorber properties and the device performance of the corresponding solar cells, and highlighting what the effect of the GGI variation is on these relationships. We investigated five CIGSe solar cells with nominal GGI ratios of 0.13, 0.34, 0.51, 0.67, and 0.83 in the CIGSe layers and analyzed these solar cells by various microscopic techniques on the identical specimen areas. It was found that the distribution of barrier heights at the grain boundaries within a specific CIGSe thin film is independent of its GGI ratio and does not influence the device performance. Compositional gradients, Urbach energy, and fluctuations in spatial luminescence distributions with increasing GGI are features that limit the radiative V_{OC} . At $GGI > 0.5$, the density of GBs and GB recombination velocity in the CIGSe thin films is large. Thus, high ΔV_{OC} is also correlated to a reduction in the effective electron lifetime due to an enhanced nonradiative recombination at these planar defects.

2 | Materials and Methods

CIGSe solar cells were prepared on soda-lime glass substrates with sputtered Mo back contacts on top. CIGSe was deposited by an in-line multi-stage co-evaporation process and the different, nominal GGI ratios were realized by adapting the Ga and In deposition rates in the first Cu-free stage at substrate heater temperatures around 450°C for 13 min and second/third stage of the process at higher substrate heater temperatures around 650°C for 13 min. In addition, all CIGSe absorbers were subject to an in-situ RbF-PDT process under Se atmosphere. More details on the CIGSe deposition process with the industry-relevant 30×30 cm² in-line coater can be found in Gutzler et al. [16]. Solution-grown CdS served as buffer layer in combination with rf-sputtered i-ZnO deposited without any additional heating as high-resistive layer. ZnO:Al window layers, which served as

conductive front contact, were dc-sputtered at a nominal temperature of 180°C with Ni/Al/Ni grid fingers on top and no anti-reflective coating was applied. The total cell area is 0.5 cm² as defined by mechanical scribing.

Current–voltage (I-V) curves were recorded with a WACOM solar simulator at standard testing conditions with a simulated AM1.5G spectrum and a Si reference cell. CIGSe solar cells were measured in the as-grown state without any further light-soaking or post-annealing procedure. X-ray fluorescence (XRF) was performed with a Fisherscope X-ray XDV-SDD on CIGSe absorbers on Mo-coated soda-lime glass substrates for determination of the integral chemical composition.

Lifetime of the minority charge carriers was obtained via time-resolved photoluminescence (TRPL) using a diode laser with a wavelength of 640 nm and a pulse frequency between 0.2 and 1 MHz together with a photomultiplier detector (H10330A-45, PMA-C). TRPL decay was acquired at room temperature on the bare CIGSe absorber layer post etching. External quantum efficiency (EQE) spectra for the determination of the bandgap and Urbach energies were acquired over a wavelength range of 300 to 1400 nm, at 10 nm steps, under an illumination spot size of 5×5 mm² and detected using a grating monochromator. EQE spectra were recorded at bias voltages of 0 V and also at −0.5 V and −1 V applying silicon and indium gallium arsenide solar cells as references.

The electron backscatter diffraction (EBSD) maps and energy dispersive X-ray spectroscopy (EDS) maps were acquired using Zeiss UltraPlus scanning electron microscopes in combination with Oxford Instruments NordlysNano. The elemental distribution maps by means of EDS were measured at an acceleration voltage of 7 kV and evaluated using Aztec software packages. The EBSD measurements for microstructure analysis were performed at a beam energy of 12–15 kV, and with a step size of 20–50 nm and evaluated using the Oxford Instruments/HKL software packages Aztec and CHANNEL5 and a pseudocubic symmetry for indexing the EBSD patterns. Cathodoluminescence (CL) spectroscopy was performed at an acceleration voltage of 10 kV and beam current of 1.2 nA over a specimen area of about 20 μm², using Zeiss Merlin scanning electron microscope equipped with DELMIC SPARC CL system [17]. The hyperspectral CL images were evaluated using the DELMIC Odemis Viewer software and the software tool Fiji.

3 | Results

3.1 | Effect of GGI on the Device Performance

Table 1 shows the photovoltaic (PV) parameters of the five investigated CIGSe thin-film solar cells. The V_{OC} increases and short-circuit current density (j_{sc}) decreases with E_g (determined from the local maximum of the first derivative of the EQE spectrum at the EQE onset), in qualitative agreement with the SQ theory [6, 7]. The fill factor (FF) and power-conversion efficiency (η) decrease substantially with increasing E_g for $GGI > 0.51$. The V_{OC} deficit $\Delta V_{OC} = (E_g/e) - V_{OC}$ (e is the elemental charge) is calculated from the difference in the corresponding E_g determined from EQE and the measured V_{OC} from the I-V characteristics.

TABLE 1 | Photovoltaic parameters and V_{OC} deficits of the five CIGSe solar cells with different GGI ratios and the band-gap energies (E_g) determined from the local maxima in the first derivatives of the EQE spectra at their absorption onsets.

Cell no.	GGI	E_g (eV)	V_{OC} (mV)	j_{sc} (mA)	FF (%)	η (%)	ΔV_{OC} (mV)
1	0.13 ± 0.03	1.09 ± 0.01	560 ± 2	34.7 ± 0.1	75 ± 1	14.9 ± 0.2	530 ± 12
2	0.34 ± 0.03	1.23 ± 0.01	730 ± 3	29.8 ± 0.1	76 ± 2	16.7 ± 0.1	500 ± 13
3	0.51 ± 0.03	1.34 ± 0.01	780 ± 3	25.5 ± 0.3	77 ± 1	15.2 ± 0.3	560 ± 13
4	0.67 ± 0.02	1.46 ± 0.01	830 ± 4	21.1 ± 0.1	71 ± 2	12.8 ± 0.2	630 ± 14
5	0.83 ± 0.03	1.58 ± 0.01	860 ± 4	14.8 ± 0.1	65 ± 2	8.3 ± 0.2	720 ± 14

Note: The given values and errors are averages and standard deviations from five individual cells.

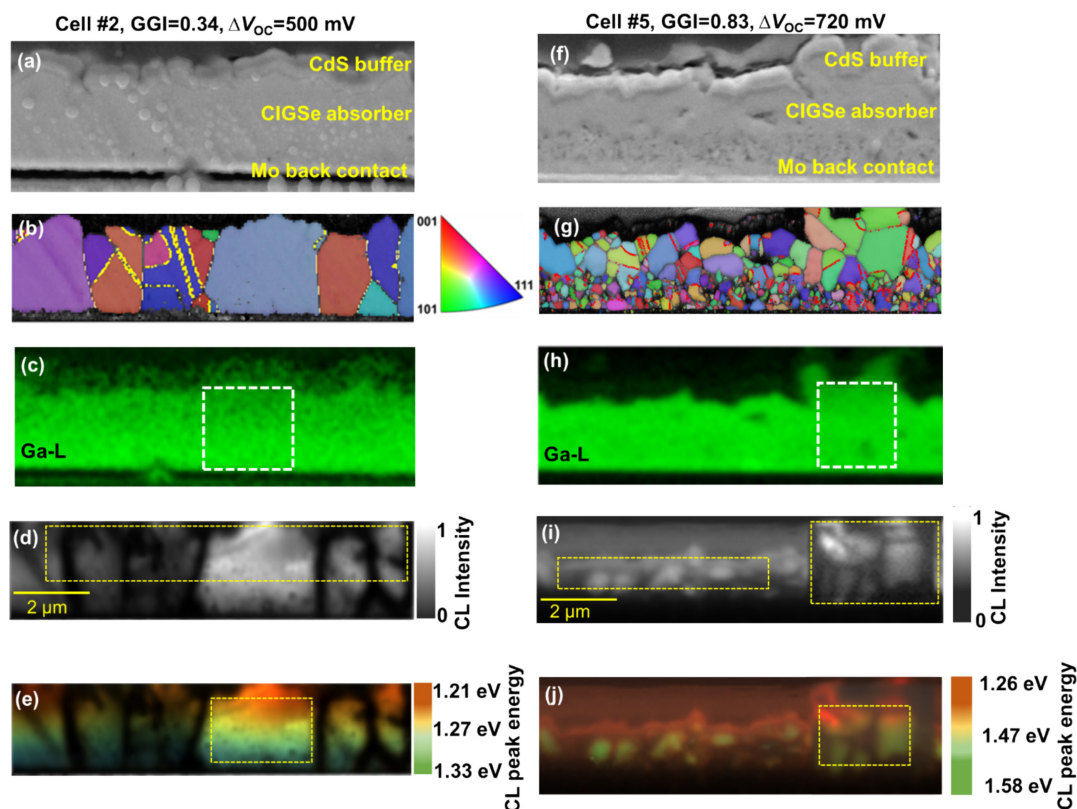


FIGURE 1 | Various microscopic results obtained from the same identical specimen areas of cross-sectional specimens of the cells #2 and #5, prepared from ZnO/CdS/CIGSe/Mo/glass stacks. (a, f) SEM images. (b, g) EBSD pattern-quality maps, showing the differences in the grain-size distributions. (c, h) Ga distribution maps (Ga-L X-ray lines) acquired by means of EDX. The highlighted regions (white, dashed rectangles) indicate the areas from where the line scans perpendicular to the substrate were extracted (Figure 2). (d, i) CL intensity distributions. The yellow, dashed rectangles indicate the regions in which GB recombination velocities were determined (Figure 5). (e, j) CL emission-energy distributions. The yellow, dashed rectangles indicate the regions from which the σ_{later} and σ_{verti} was calculated.

ΔV_{OC} is 530 mV at GGI = 0.13 decreases to a minimum of 500 mV for cell #2 with GGI 0.34 and then increases with increasing GGI. Cell #5 with the largest nominal GGI of 0.83 exhibits the highest ΔV_{OC} of 720 mV. To understand possible origins of ΔV_{OC} , it is necessary to study the effect of GGI variation on various material properties and relate these properties to the ΔV_{OC} as shown in the following subsections. Further origins than those addressed in the present work have to be considered, for example, properties of interfaces between absorber and contacts that change with varying GGI that can be characterized, for example, via impedance and surface voltage spectroscopy [18, 19]. In the present work, we focus on the material properties on

the sub-micrometer scale, characterized via correlative SEM techniques.

3.2 | Microstructural, Compositional, and Luminescence Properties of the CIGSe Layers

We assessed various microscopic properties, via acquiring EBSD, EDX, and CL maps on identical positions of individual CIGSe absorbers with varying GGI as shown in Figure 1. Cell #2, with a nominal GGI of 0.34, exhibits the smallest ΔV_{OC} of 500 mV, while cell #5 features the highest nominal GGI of 0.83

and a large ΔV_{OC} of 720 mV. We take a closer look into the structure–property relationships, by comparing various properties of the two cells with the highest and moderate GGI values of 0.83 and 0.34 and further study the effect of these properties on the corresponding ΔV_{OC} (the correlative electron microscopy results of the three other solar cells with GGI values of 0.13, 0.51, and 0.67 are provided in Figures S1, S2, and S3).

Figure 1 shows a comparison of the microstructures from EBSD maps (Figure 1b,g), the Ga distributions via EDX (Figure 1c,h), and the lateral distributions of the luminescence emission using CL (Figure 1d,i,e,j) of the two cells.

The EBSD maps in Figure 1b,g depict the differences in the grain sizes at two different GGI ratios of 0.34 and 0.83. EBSD maps were acquired on consecutive regions with a point-to-point distance of 20–50 nm. We define the diameter of an individual grain as the one of a circle that has the same area as this grain. The average grain size d_{grain} is the average of the equivalent circle diameters extracted from the EBSD maps with more than 200 grains (the maps in Figure 1 are only sections of much larger EBSD maps). Although, strictly speaking, grain sizes in CIGSe layers exhibit a lognormal distribution [20], we assumed a Gaussian distribution to calculate the average grain size. No preferred local orientation

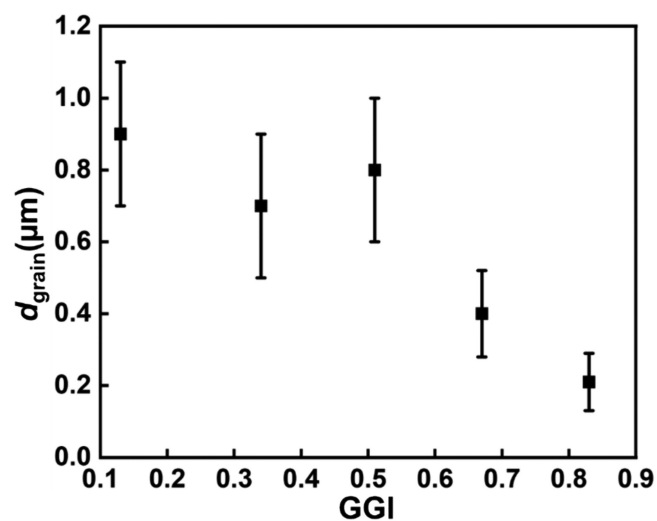


FIGURE 2 | Average grain sizes vs. GGI, showing a substantial decrease in the grain size as the GGI increases.

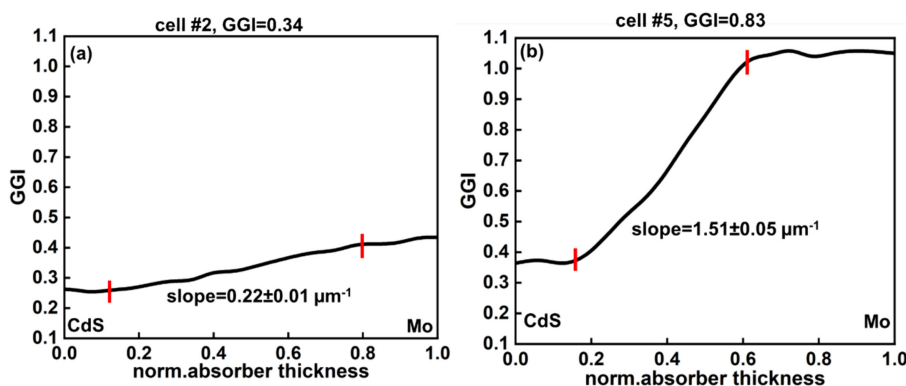


FIGURE 3 | GGI gradients extracted from the EDS maps of the CIGSe absorbers. (a) GGI gradient for cell #2, GGI=0.34. (b) GGI gradient for cell #5, GGI=0.83. The slope was estimated by fitting the range in the gradient that are marked in red.

was detected (Supplementary information Figure S4). The EBSD maps were also used to localize and classify the grain boundaries (GBs). Cell #5 with GGI of 0.83 features a higher density of GBs owing to the smaller size of the grains.

From Figure 2, it is evident that the changes in the nominal GGI have a substantial impact on d_{grain} . The d_{grain} steadily decreases as the GGI approaches more higher ratios of 0.83. For this GGI ratio, the d_{grain} in the CIGSe layer is only about $0.2\mu\text{m}$, which is the smallest among all the five CIGSe solar cells. While at smaller GGIs of 0.13 and 0.34, the CIGSe layer is composed of larger grains, with d_{grain} on the order of 0.9 and $0.7\mu\text{m}$. This result is consistent with an earlier work by Abou-Ras et al., which shows a similar trend of decreasing grain size with increasing GGI [21].

From the EDX maps in Figure 1c,h, line scans were extracted perpendicular to the substrate. The GGI profiles were determined via calibrating with the integral [Ga] and [In] from the XRF measurements (see Table S1 for the XRF results). The absorber layer of cell #2 is made of large grains, uniformly distributed across the absorber layer ($d_{grain} = 0.7\mu\text{m}$) (Figure 1b). The size of the grains does not vary significantly from top to bottom of the CIGSe layer owing to a nearly flat GGI gradient with a slope of $0.22\mu\text{m}^{-1}$, as seen in Figure 3a. In contrast, cell #5 contains a CIGSe layer composed of smaller grains ($d_{grain} = 0.2\mu\text{m}$), and their sizes decrease from the CIGSe/CdS to the Mo/CIGSe interface (Figure 1g). It can be seen in Figure 1g that the sizes of the grains are larger close to the CdS buffer layer and smaller near the Mo back contact. This spatial distribution of grain sizes correlates well with a high [Ga] close to the Mo back contact and a small [Ga] near the CdS buffer layer, while the GGI gradient exhibits also a large slope of $1.51\mu\text{m}^{-1}$, as seen in Figure 3b (the slope was estimated by fitting the linear region of the gradient, marked in red). GGI gradient of cell #1, #3, and #4 is given in Figure S5a–c.

The Ga/In gradient and the GB density influence the luminescence properties of the corresponding cells. The E_g of the absorber is dependent on the GGI via the relation $E_g(x) = (1-x)E_g(\text{CuInSe}_2) + xE_g(\text{CuGaSe}_2) - bx(1-x)$, where $x = \text{GGI}$ and $b = 0.2$ is the optical bowing parameter [2]. The E_g gradient within the absorber should exhibit a similar distribution perpendicular to the substrate as that of the GGI gradient. Indeed, the luminescence energy distributions of the CIGSe layers in Figure 1e,j confirm the presence of a linear E_g gradient within the absorber depth.

In Figure 1e,j, the CL peak energies from the CIGSe absorber vary significantly both, in parallel and in perpendicular directions with respect to the substrate. This result is an indication that fluctuations in the luminescence energy distribution are present in both directions. These fluctuations were quantified from the standard deviations of the luminescence energy distribution across 32 pixels from homogenous regions highlighted in Figure 1e,j. The quantities σ_{lateral} and σ_{verti} are the luminescence fluctuations determined in parallel and perpendicular directions to the substrate with a spatial resolution of 50–70 nm. Cell #5 exhibits higher fluctuation values (Figure 1j) in the range of 3–60 and 80–105 meV, than those for cell #2, about 2–11 and 30–38 meV (Figure 1e).

3.3 | Recombination at GBs

Figure 1d,i shows the luminescence intensity distributions. It is visible clearly that the CL intensity is higher within the grain interiors, but that the intensity decreases strongly towards the GBs. Such variation in the CL intensity is an indication of non-radiative recombination of electrons at these GBs. For the quantification of this recombination, line scans across about 20 GBs for each cell were extracted from the corresponding CL intensity distribution maps (Figure 1d,i). Because extracting these line scans requires sufficiently large grains on either side of the GB (diameters of few 100 nm), only regions with correspondingly large grains were evaluated (highlighted by yellow, dashed rectangles in the Figure 1d,i).

GB recombination velocities at individual GBs (S_{GB}) are determined based on the approach proposed by Mendis et al. [22, 23], which fits the logarithm of the CL intensity gradient $\ln[\Delta I(x)]$ by the linear function $\ln[S/(S+1)] - x/L$. Here, x is the position of the electron beam, L is the electron diffusion length, S is the reduced recombination velocity with $S = S_{\text{GB}}\tau_{\text{bulk}}/L$ (τ_{bulk} is the bulk lifetime of electrons). The CL intensity linescans and the corresponding linear fits for cell #5 with the highest GGI and smallest d_{grain} are provided in the supporting information in Figure S6. An extension of this approach adapted to CIGSe absorbers is detailed in Krause et al. [24]. In order to calculate the recombination velocity S_{GB} , the bulk lifetime of electrons, τ_{bulk} , is needed. We did not measure this quantity directly but obtained it indirectly via the following procedure.

For the five CIGSe thin-films, TRPL measurements were performed on bare absorber layers immediately after etching (Figure 4a–e). From Figure 4a–e, it is apparent that the TRPL curves cannot be described by one exponential function only. Rather, these dependencies exhibit two sections: one with a faster decay time τ_1 and one with a slower decay time τ_2 . Therefore, the TRPL decay for each CIGSe absorber was fitted using a bi-exponential function of the form $y(x) = A_1 \exp(x/\tau_1) + A_2 \exp(x/\tau_2)$ (Figure 4a–e, red) [25, 26].

There are numerous effects that may cause such bi-exponential decay. The most likely ones are charge-carrier trapping at flat defects [27], distinct surface recombination [28], and charge separation within a (weak) electric field due to potential fluctuations [29]. As the interpretation of the decay time is different in each of these cases, the dominating effect has to be unveiled first using a laser intensity variation [30]. By increasing the laser excitation,

we found a decrease of the second decay time τ_2 , while the first component is almost unaffected (see Figure S7 and Table S2). This is in contradiction to what can be expected for charge separation and charge carrier trapping. Therefore, the TRPL signal is governed by recombination in the bulk and at the (grain) surfaces. In this case, τ_2 approximates the effective recombination lifetime τ_{eff} , and we set τ_2 to τ_{eff} in the following evaluations.

We selected those τ_2 lifetimes that were measured at the lowest laser intensity (see Section S9 in the supporting information for details), in order to remain under low-injection conditions [31]. As apparent from Table S2, the highest τ_{eff} of about 760 ns was also found for the best performing cell #2, in which the CIGSe layer exhibits a GGI ratio of 0.34. The lowest τ_{eff} was measured for cell #5, for which the average grain size also was smallest.

The recombination of the charge carriers is dependent on the lifetime of the electrons. Based on Matthiesen's rule, the inverse of the effective electron lifetime is related to the radiative component of the electron lifetime in the bulk ($\tau_{\text{rad,bulk}}$) in addition to the lifetime components of nonradiative recombination in the bulk ($\tau_{\text{nonrad,bulk}}$), at the front/back interfaces ($\tau_{\text{interfaces}}$) as well as at grain boundaries (τ_{GB}) and any dislocations ($\tau_{\text{dislocations}}$) [32]:

$$\tau_{\text{eff}}^{-1} \approx \tau_{\text{rad,bulk}}^{-1} + \tau_{\text{nonrad,bulk}}^{-1} + \tau_{\text{interfaces}}^{-1} + \tau_{\text{dislocations}}^{-1} + \tau_{\text{GB}}^{-1} \quad (1)$$

The PL decay obtained on the bare CIGSe absorbers does not include any effects from recombination at the CIGSe/Mo back interface, as the luminescence emission is most effective from the region of the lowest band-gap energy, which for all CIGSe layers is situated closer to the CIGSe surface (visible in the GGI distributions in Figures 3 and S5). However, a contribution from the recombination near the CIGSe surface to τ_{eff} cannot be excluded. Nevertheless, it is convenient to simplify Equation (1) in order to have only contributions from the lifetime in the bulk and from the lifetime at the GBs:

$$\tau_{\text{eff}}^{-1} \approx \tau_{\text{bulk}}^{-1} + \tau_{\text{GB}}^{-1} \quad (2)$$

We keep in mind that because of the considerations above, τ_{bulk} contains not only the contributions from recombination in the bulk, but also those from the CIGSe surface (relevant) and those from dislocations (probably negligible [33]). Moreover, we note that the TRPL decay may be affected by several factors such as carrier detrapping and lateral inhomogeneities [27]. Therefore, the estimated bulk lifetimes and the corresponding GB lifetimes feature large errors that are of the same order of magnitude as the estimated values.

In order to determine τ_{bulk} , we need to estimate τ_{bulk} and τ_{GB} for a given τ_{eff} (which is equal to the τ_2 value from TRPL measurements, as already explained above) via Equation (2) for each of the five cells such that $\tau_{\text{bulk}} \geq \tau_{\text{GB}}$ and $\tau_{\text{bulk}} \geq \tau_{\text{eff}}$. These roughly estimated τ_{bulk} are used as input in evaluation of the CL intensity profiles using the relationship $S = S_{\text{GB}}\tau_{\text{bulk}}/L$ to calculate all S_{GB} values from one sample. Secondly, the median value of all S_{GB} values from each sample, $S_{\text{GB},0}$, which is obtained by assuming a specific τ_{bulk} in the evaluation of the CL intensity profiles, must fulfill [34–37].

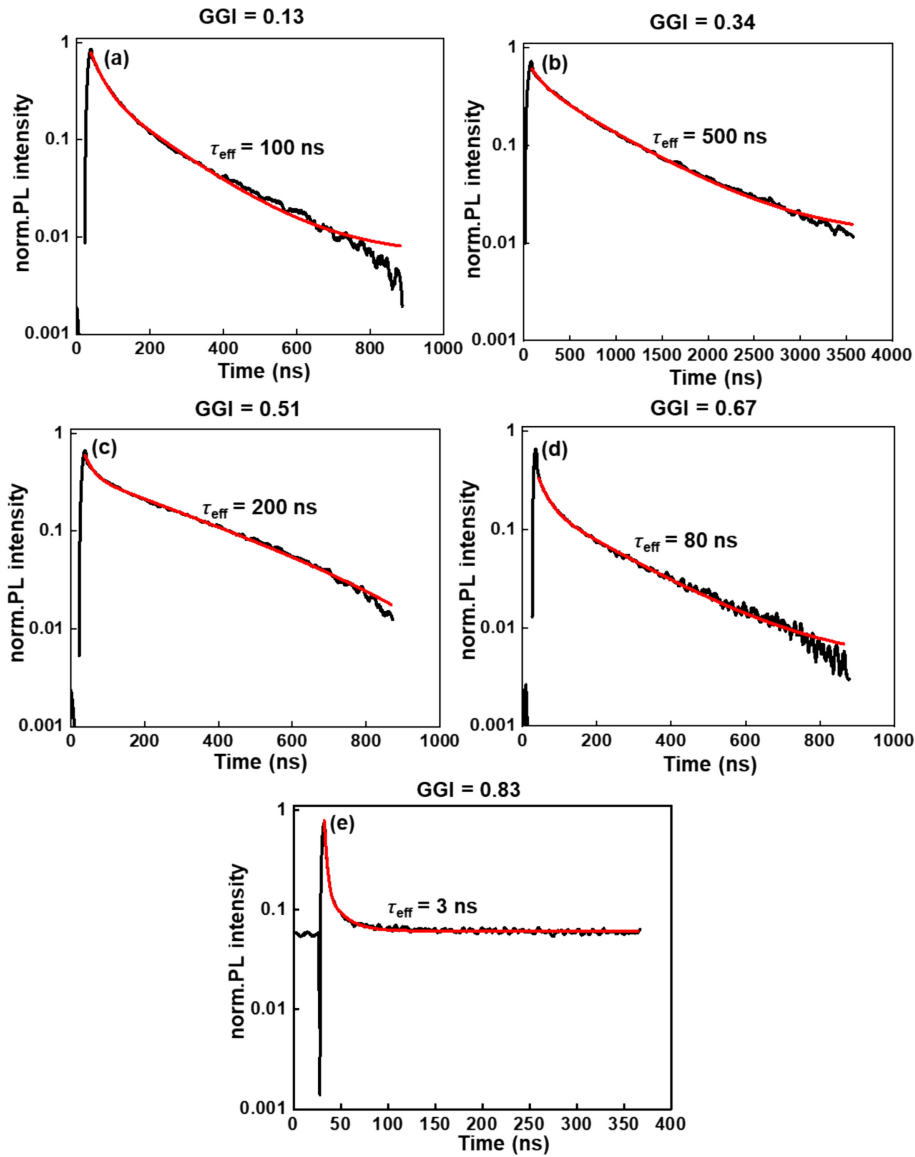


FIGURE 4 | (a–e) TRPL decays of all the five CIGSe absorbers with different GGI, acquired at 10% laser intensity (black lines), as well as the bi-exponential fits of these decays (red lines).

$$\tau_{\text{GB}} = d_{\text{grain}} / (6 - n) S_{\text{GB},0} \quad (3)$$

Here, d_{grain} is the average grain size determined by EBSD analyses. For the estimate of Equation (3), we consider cubical shapes for the grains in the polycrystalline CIGSe absorber [32]. In Equation (3), n is the number of passivated faces among the six faces of an assumed, cubically shaped grain. The extent of the passivation at the GB planes was not determined in the present work for neither of the five samples; because GB planes in CIGSe are, per se, not passivated [38], we set $n=0$ in Equation (3). The GB lifetime τ_{GB} calculated from Equation (3) must be (nearly) equal to the assumed τ_{GB} in Equation (2) and always greater than τ_{eff} .

The resulting values of τ_{bulk} , τ_{GB} and τ_{eff} for all samples are listed in Table S3. It should be noted that the calculated τ_{GB} values do not change substantially when assuming $n=0$ or $n=1$ in Equation (3) (i.e., assuming none or one passivated face of the grain, e.g., the

one at the CdS/CIGSe interface). These lifetime values are rough estimates, that is, the errors of τ_{bulk} , τ_{GB} , and τ_{eff} are on the same order of magnitude as their individual values. τ_{bulk} is an effective lifetime of the electrons in the bulk, and the large τ_{bulk} values indicate that the contribution of surface recombination does not differ much from that of the bulk; we note that the τ_{bulk} values given in the present work are overestimated and that the real at least one order of magnitude smaller, limited by the radiative lifetime. Nevertheless, from the comparison of the TRPL decays of the five CIGSe thin-film solar cells, it is clear that the lifetimes τ_{eff} , τ_{bulk} , and τ_{GB} increase with increasing GGI from GGI=0.13 to 0.34 and then decrease for the higher GGI values. It should be considered that cells #4 and #5 with high GGIs of 0.67 and 0.83 may have a cliff-like conduction-band offset, causing an enhanced recombination at the CdS/CIGSe interface; however, in the present case, τ_{eff} is calculated from TRPL measured on bare CIGSe absorbers (on Mo/glass substrates), and therefore, the effects from recombination at the CdS/CIGSe interfaces recombination can be neglected.

The recombination velocities S_{GB} determined by the approach described above exhibit a strong variation from 1 GB plane to another within an individual CIGSe absorber (black squares in Figure 5a,b). This difference in the S_{GB} values from 1 GB to another within the same CIGSe absorber is also an indication for that the CL maps were acquired under low injection conditions (without any additional charge carriers being generated). Else, the GBs would have exhibited much larger and similar S_{GB} values on the order of 10^3 – 10^5 cm/s, as reported and discussed in Refs. [39, 40]. These values vary from about 2 to 140 cm/s at GGI of 0.34 and from about 2 to 380 cm/s for the CIGSe absorber with GGI=0.83. Brody and Rohatgi [41] suggested for the recombination velocities at semiconductor surface the following expression, which we transfer to GBs as internal surfaces:

$$S_{GB} = N_{GB} \sigma_{GB} v_{th} \exp(-\phi_b/k_B T) \quad (4)$$

Here, N_{GB} , σ_{GB} , and v_{th} are the point-defect concentration at the GB plane, their effective capture cross-section for electrons, as well as the thermal velocity of electrons, while k_B and T are the Boltzmann constant and the absolute temperature. It is noted that Equation (3) can also be obtained when using the equation for the barrier height proposed by Seto (equation 9 in Seto [42]) in the S_{GB} equation suggested by Seager (equation 33 in Seager [43]). We assume that the prefactor $N_{GB} \sigma_{GB} v_{th}$ describing the nonradiative Shockley–Read–Hall recombination at a GB plane does not vary by more than one order of magnitude at the various GBs in a polycrystalline CIGSe layer; this assumption makes sense when regarding the substantial interdiffusion at the elevated temperatures used for the synthesis of the CIGSe layers, leading to correspondingly (quasi)homogeneous segregation and spatial distributions of these point defects at GBs (not saying that the densities of these point defects are identical at different GBs). Consequently, the effective defect density and its effective capture cross-section can be expected to differ only within the same order of magnitude from GB to GB. We set the median value as an effective recombination velocity for all GBs in an individual CIGSe layer. Given the inaccurate nature of Equation (5), the error for $S_{GB,0}$ is large (same order of magnitude as the $S_{GB,0}$ value).

$$S_{GB,0} \approx N_{GB} \sigma_{GB} v_{th} \quad (5)$$

To simulate the measured recombination velocities S_{GB} in Figure 5 using Equation (3), we only need to assume various barrier heights ϕ_b using the corresponding median value $S_{GB,0}$. For barrier heights ranging from several -10 meV to several $+10$ meV, it is indeed possible to reproduce theoretically (red circles in Figure 5a,b) the experimental S_{GB} values in Figure 5a,b (results from cells #1, #3, and #4 are provided in Figures S7, S8, and S9).

Using the expression $\phi_b = k_B T \ln(S_{GB,0}/S_{GB})$ (from Equations 3 and 5), the barrier heights for all GBs and all samples were calculated and depicted in Figure 6. This viewgraph indicates that the GGI variation has no considerable effect on the range of the assumed ϕ_b values. This result can be expected when assuming that independent of the GGI, the effective (positive or negative) net-charge densities at various GBs within the identical CIGSe layer are always different, because the ensembles of point defects contributing to the total defect densities at these GB planes are always different.

The median value $S_{GB,0}$ decreases first from GGI=0.13 to GGI=0.34 with increasing GGI and then increases for higher GGI ratios, remaining at the same level for GGI=0.51–0.83 (Figure 7). Cell #2 with GGI=0.34 with the highest conversion efficiency and relatively low ΔV_{OC} exhibits the lowest $S_{GB,0}$ of about 15 cm/s.

3.4 | Effect of the GGI Ratio on the Spatial Luminescence Distribution and the Urbach Energy

Figure 8a indicates that for increasing GGI ratio, the maximum value of the lateral luminescence variation, σ_{later} (black), increases from 5 to 60 meV, and also the maximum value of the vertical luminescence variation, σ_{verti} (red), increases from 14 to 105 meV (the σ_{verti} value for GGI=0.34 deviates slightly from this trend).

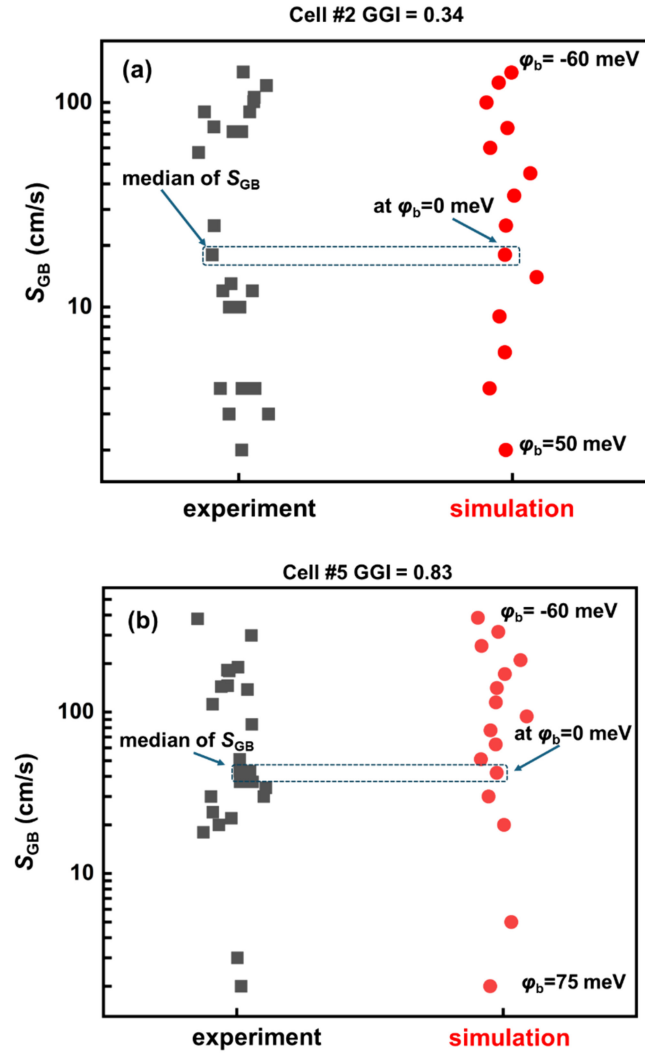


FIGURE 5 | (a) Experimental (black square) and simulated (red circle) GB recombination velocities of cell #2 with GGI=0.34 based on Equation (3) by assuming a constant $S_{GB,0}$ and varying only ϕ_b . The assumed barrier heights extend over a range from -60 to 50 meV. (b) Experimental (black square) and simulated (red circle) S_{GB} for CIGSe solar cell #5, GGI=0.83 based on Equation (3) by assuming a constant $S_{GB,0}$ and varying only ϕ_b . The barrier heights range from -60 to 75 meV. The individual data points are shifted in left and right directions to avoid overlaps of the data points and thus, to provide better visibility. The error in every individual S_{GB} is of the same order of magnitude of that corresponding S_{GB} .

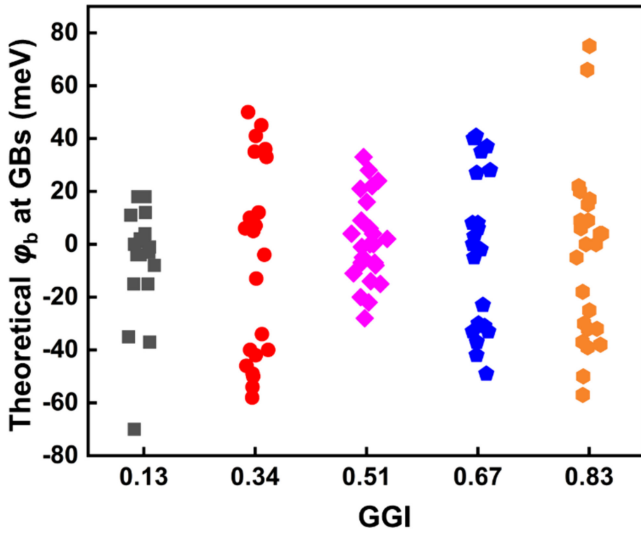


FIGURE 6 | Distribution of barrier heights φ_b used for S_{GB} simulation for each of the five CIGSe thin-film solar cells with different GGI. Majority of the assumed φ_b is distributed nearly within the same interval, showing no specific trend in the φ_b distribution with respect to the GGI variation.

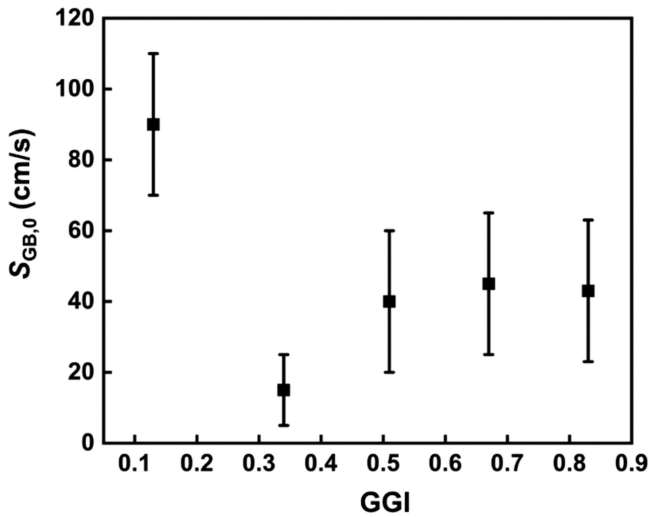


FIGURE 7 | Median of GB recombination velocity $S_{GB,0}$ vs. GGI ratio.

We note that always, $\sigma_{\text{verti}} > \sigma_{\text{later}}$. The Ga/In gradients present in CIGSe layers were identified as main effect on σ_{verti} [44].

We also determined the Urbach energies E_u by evaluation of the subgap region at the EQE onset for all five CIGSe solar cells based on the approach described in Ref [45]. Figure S10a shows the corresponding EQE spectra. As shown in Figure 8b (black squares), E_u also increases with increasing GGI. The lattice parameters c and a of the tetragonal crystal structure were calculated at specific GGI ratios using the approach detailed in Balboul et al. [8]. It was shown by Abou-Ras et al. [21] that the c/a ratio increases first with increasing GGI ratio up to a GGI ratio of 0.23 (for which $c/a = 2$), and then decreasing for larger GGI ratios. The decrease in lattice constant a with the increasing GGI is also directly linked to an increase in the anion displacement parameter u [46, 47]. Thus, the higher the value of u , the larger is the tetragonal distortion,

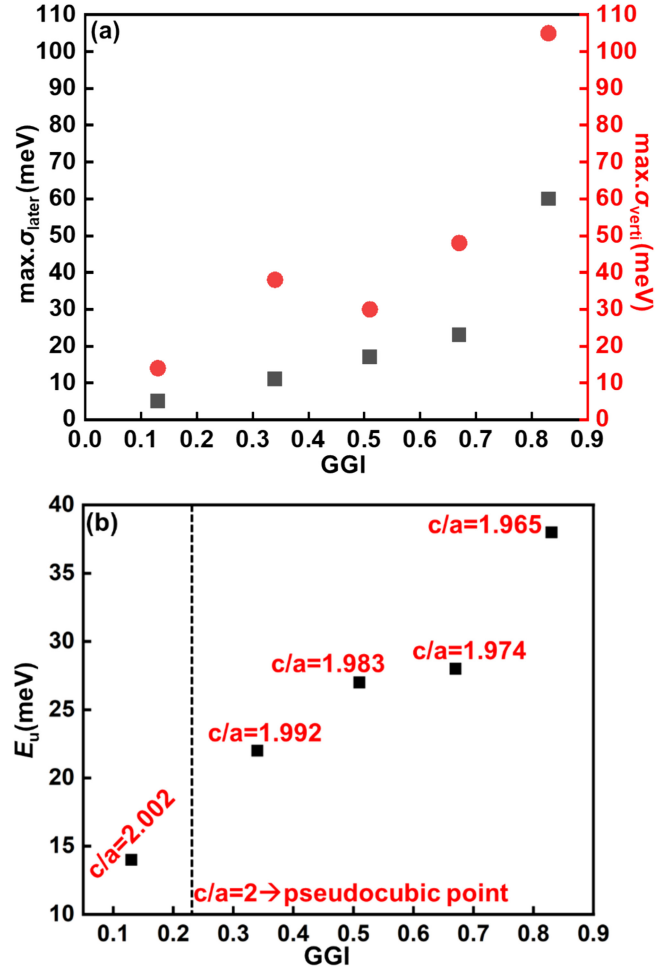


FIGURE 8 | (a) Maximum lateral and vertical CL emission fluctuations vs. GGI. Both $\max.\sigma_{\text{verti}}$ (red) and $\max.\sigma_{\text{later}}$ (black) increase with GGI variation. (b) E_u vs. GGI, where E_u (black) increases with increasing GGI and decreasing c/a (red). Dashed black line indicates $\text{GGI}=0.23$, at which the lattice pseudocubic point $c/a=2$ is present.

inducing changes in the electronic band structure. Therefore, the changes in crystal structure, directly influences the range of energy levels of the electrons characterized by E_u . In addition, the larger the deviation of c/a from 2 (pseudocubic), the larger is the strain contained in the thin film. This strain can be linked to local variations of subgap states represented by E_u and thus, also with the lateral luminescence variation σ_{later} . Indeed, E_u correlates well with σ_{later} (Figure S10b).

4 | Discussion

As outlined in Table 2, the average grain size d_{grain} , the electron lifetime τ_{eff} , τ_{GB} , GB recombination velocity $S_{GB,0}$, the fluctuations in CL emission (σ_{later} , σ_{verti}) as well as the Urbach energy (E_u) are all affected considerably by the GGI variation. The changes in these material properties have a substantial impact on the ΔV_{oc} . In order to organize the discussion of these results, it is convenient to divide them into those material properties whose changes induce radiative (σ_{later} , σ_{verti} , E_u) and those that lead to nonradiative V_{oc} losses (τ_{bulk} , d_{grain} , τ_{GB} , $S_{GB,0}$).

TABLE 2 | Various material and device properties of the CIGSe layers and cells: the V_{OC} deficit (ΔV_{OC}), radiative V_{OC} deficit (ΔV_{OC}^{rad}), nonradiative V_{OC} deficit (ΔV_{OC}^{nonrad}), the average grain size (d_{grain}), the effective electron lifetime (τ_{eff}), the bulk lifetime (τ_{bulk}), the electron lifetime at GBs (τ_{GB}) assuming no passivated facets ($n=0$), the GB recombination velocity ($S_{GB,0}$), luminescence fluctuations (σ_{vert} , σ_{later}), the slope in the Ga/In gradient, and the Urbach energy (E_u).

GGI	ΔV_{OC} (mV)	ΔV_{OC}^{rad} (mV)	ΔV_{OC}^{nonrad} (mV)	d_{grain} (μm)	τ_2 (ns)	τ_{bulk} (ns)	τ_{GB} (ns)	$S_{GB,0}$ (cm/s)	$\sigma_{verti.}$ (meV)	Slope in Ga/ In gradient		E_u (meV)
										(μm^{-1})	(meV)	
0.13	530	50	480	0.9	160	3500	170	90	12–14	0.03	2–5	14
0.34	500	45	455	0.7	760	25,000	780	15	30–38	0.22	2–11	22
0.51	560	40	520	0.8	320	14,000	320	40	21–30	0.19	2–17	27
0.67	630	65	565	0.4	140	13,000	140	45	11–48	2.1	4–23	28
0.83	720	50	670	0.2	80	1700	80	40	80–105	1.5	3–60	36

4.1 | Radiative V_{OC} Losses

As shown by Rau et al. [48], the broadening of the onset of the absorption or EQE spectrum of a semiconductor material or the corresponding solar-cell device is correlated directly with shifts of the luminescence peak from the band-gap energy (calculated from the local maximum in $dEQE/dE$). This correlation has recently been verified for about 30 CIGSe solar cells with various compositions and growth recipes [49]. Therefore, the corresponding quantities E_U (as a measure for different slopes in the subgap regions at the onsets of the absorption spectrum) and $\sigma_{later}/\sigma_{verti}$ (quantifying emission-peak shifts) can be expected to be connected. As shown by Rau et al. [50], a broadening of the onset of the absorption or EQE spectrum (σ_g) can be translated into a corresponding radiative V_{OC} loss via $\Delta V_{OC}^{rad} = \sigma_g^2/2k_B T$. In the present work, the ΔV_{OC}^{rad} values are of the order of 40–65 mV (Table 2), which are much lower than the ΔV_{OC}^{nonrad} values (see below).

In all five CIGSe layers (cells #1–#5), Ga/In gradients are present. As visible from a comparison of the slopes in the gradients and the σ_{verti} values in Table 2, they correlate well for the GGI range of 0.13–0.51. For GGI=0.67 and 0.83, this correlation is not given anymore. An explanation for this behavior is given by the microstructures of the five CIGSe layers (EBSD maps in Figures 1 and S4). For GGI=0.13, 0.34, and 0.51, many grains extend from the back to the front contact. Thus, only the strain present due to the Ga/In gradient extending across the entire grain contributes to σ_{verti} . However, for GGI=0.67 and 0.83, the average grain sizes are much smaller than the CIGSe layer thicknesses, and thus, additional strain fields at and around the GBs have to be taken into account. Because for cell #5, the σ_{verti} value is much larger than the one for cell #4, although the slope of the Ga/In gradient is smaller for cell #5 than that for cell #4, it seems that the average grain size has a stronger impact on the local variation of the luminescence peak energy in vertical direction than the slope in the Ga/In gradient.

It is well visible in Table 2 (and also in Figure 8b) that the trend of increasing E_U with increasing GGI ratio agrees well with the likewise enhancing lateral fluctuation in the CL emission energy σ_{later} . The anion displacement parameter u depends on the lattice constant and the cation-anion bond lengths. In Ref [51], it is shown that the u deviates from the ideal value of 0.25, as a

function of the $[In]/([In] + [Ga])$ ratio (i.e., the GGI ratio). This dependency of u on the composition is also applicable in the present work. As shown in Figures 8b and S10c, the deviation of c/a from the corresponding value of 2 at the pseudocubic point, $|c/a-2|$, increases with increasing GGI from 0.13 to 0.83. This indicates that there is also similar deviation in u as a function of GGI, following the dependency of u on the lattice constant a . These deviations in c/a and u introduces an additional strain in the CIGSe thin film, leading to alterations in subgap states which seems to be connected with σ_{later} and E_U . We should note that strain due to a deviation of $c/a=2$ can be expected to be present also perpendicular to the substrate. However, as always $\sigma_{verti} \gg \sigma_{later}$, the contribution of this specific strain to σ_{verti} is negligible (i.e., the effect of the Ga/In gradients is dominant in the vertical direction).

4.2 | Nonradiative V_{OC} Losses

Nonradiative V_{OC} losses (ΔV_{OC}^{nonrad}) are obtained from $\Delta V_{OC} - \Delta V_{OC}^{rad}$, as given in Table 2, and are much larger than the radiative V_{OC} losses. Auger recombination can be neglected in CIGSe thin-film layers owing to the net-doping density of about 10^{15} – 10^{16} cm^{-3} . The bulk lifetime τ_{bulk} of the electrons is the highest in the CIGSe absorber of cell #2 with GGI=0.34 and $E_g=1.2$. From GGI=0.13 to 0.34, τ_{bulk} increases first and then decreases to a minimum of 10 ns for higher GGI. This trend in the electron bulk lifetime can be explained by the trend in the effective defect concentration in the CIGSe bulk, N_T , which has been shown to decrease for increasing GGI up to a GGI ratio from 0 to about 0.3, and then increasing again for larger GGI ratios [14]. As $\tau_{bulk} = (N_T \sigma_T v_{th})^{-1}$, with σ_T and v_{th} being the effective capture cross-section of the bulk defects and the thermal velocity of the electrons, an increase (decrease) in N_T leads to a decrease (increase) in τ_{bulk} . However, we find that for all CIGSe layers (Table 2), τ_{eff} is closer to τ_{GB} than to τ_{bulk} . Therefore, the enhanced nonradiative recombination via defect states in the CIGSe bulk can be expected to contribute only slightly to ΔV_{OC}^{nonrad} .

Smaller average grain sizes d_{grain} of $< 0.5 \mu m$, as detected for the cells #4 and #5 (GGI=0.67 and 0.83) are equivalent to higher GB densities. Thus, enhanced nonradiative recombination at these planar defects can be expected that are further origins of ΔV_{OC}^{nonrad} [52]. Therefore, the increase in ΔV_{OC}^{nonrad} with GGI

partly contributes to a smaller FF at $GGI > 0.5$. As mentioned above, for all of the CIGSe layers, $\tau_{\text{eff}} \approx \tau_{\text{GB}}$ (Table 2), that is, a major contribution to $\Delta V_{\text{OC}}^{\text{nonrad}}$ comes from GB recombination. When considering that defects detected at the GB plane segregate to the planar defect from the bulk, and that therefore, τ_{GB} scales with τ_{bulk} (or the defect density at a GB, N_{GB} , with N_{T}), the trend of τ_{GB} and of the corresponding $\Delta V_{\text{OC}}^{\text{nonrad}}$ with increasing GGI can be attributed to the GGI dependency of τ_{bulk} . Similar median values $S_{\text{GB},0}$ for $GGI = 0.51$ – 0.83 indicate that the nonradiative recombination at the GBs does not change anymore for $GGI > 0.5$; the lifetime in the absorber layers is affected mainly by the different average grain sizes d_{grain} . Although the $S_{\text{GB},0}$ values are different for the five CIGSe layers, the ranges of the barrier heights at GBs are very similar, independent of the GGI ratio.

5 | Conclusions

In the present work, we investigated the effect of the GGI variation in polycrystalline CIGSe absorber layers on the various CIGSe materials properties and their impacts on the radiative and nonradiative V_{OC} losses. It was found that independent of the GGI value, lattice strain due to Ga/In gradients perpendicular to the substrate induces substantial fluctuations in the CL emission energy lead to corresponding radiative V_{OC} losses. However, the radiative V_{OC} losses are much smaller than the nonradiative V_{OC} losses, which result mainly from GB recombination. The nonradiative V_{OC} losses due to enhanced recombination at the GBs can be decreased partly in CIGSe thin-film solar cells by designing absorbers with smaller GB density (larger grains) via higher deposition temperatures and/or Ag incorporation. The trend of increased V_{OC} losses for solar cells with $GGI > 0.5$ in the CIGSe layers can be traced back to decreased bulk lifetime and to the enhanced GB recombination, which is affected by both, decreased average grain sizes and increased recombination velocities. The ranges of the estimated barriers at GBs do not exhibit any significant changes with varying GGI ratios, in contrast to the median values of recombination velocities.

Author Contributions

Main author and microscopic analyses: Sinju Thomas. Sample preparation and writing: Wolfram Witte. Sample preparation and writing: Dimitrios Hariskos. Sample preparation and writing: Rico Gutzler. Sample preparation and writing: Stefan Paetel. TRPL analysis and writing: Chang-Yun Song. TRPL analysis and writing: Heiko Kempa. TRPL analysis and writing: Matthias Maiberg. Corresponding author and supervision of the work: Daniel Abou-Ras.

Acknowledgements

The authors are grateful to Ulrike Bloeck (HZB) for assistance with the cross-sectional specimen preparation for SEM. The present work was supported by the Graduate School “MatSEC” and the project “EFFCIS-II” funded by the Federal Ministry for Economic Affairs and Climate Action (BMWK) under contract numbers 03EE1059A (ZSW), 03EE1059B (HZB), and 03EE1059C (MLU). Open Access funding enabled and organized by Projekt DEAL.

Data Availability Statement

The data that support the findings of this study are available from the corresponding author upon reasonable request.

References

1. M. Nakamura, K. Yamaguchi, Y. Kimoto, Y. Yasaki, T. Kato, and H. Sugimoto, “Cd-Free Cu (In,Ga)(Se,S)₂ Thin-Film Solar Cell With Record Efficiency of 23.35%,” *IEEE Journal of Photovoltaics* 9, no. 6 (2019): 1863–1867.
2. W. Hörig, H. Neumann, H. Sobotta, B. Schumann, and G. Kühn, “The Optical Properties of CuInSe₂ Thin Films,” *Thin Solid Films* 48, no. 1 (1978): 67–72.
3. W. Hörig, H. Neumann, B. Schumann, and G. Kühn, “Optical Properties of CuGaSe₂ Near and Above the Fundamental Absorption Edge,” *Physica Status Solidi B: Basic Solid State Physics* 85 (1978): 57–61.
4. T. Feurer, R. Carron, G. Torres Sevilla, et al., “Efficiency Improvement of Near-Stoichiometric CuInSe₂ Solar Cells for Application in Tandem Devices,” *Advanced Energy Materials* 9, no. 35 (2019): 2–7.
5. M. Jošt, E. Köhnen, A. Al-Ashouri, et al., “Perovskite/CIGS Tandem Solar Cells: From Certified 24.2% Toward 30% and Beyond,” *ACS Energy Letters* 7, no. 4 (2022): 1298–1307.
6. W. Shockley and H. J. Queisser, “Detailed Balance Limit of Efficiency of p-n Junction Solar Cells,” *Journal of Applied Physics* 32, no. 3 (1961): 510–519.
7. S. Rühle, “Tabulated Values of the Shockley-Queisser Limit for Single Junction Solar Cells,” *Solar Energy* 130 (2016): 139–147.
8. M. R. Balboul, H. W. Schock, S. A. Fayak, A. A. El-Aal, J. H. Werner, and A. A. Ramadan, “Correlation of Structure Parameters of Absorber Layer With Efficiency of Cu(In,Ga)Se₂ Solar Cell,” *Applied Physics A: Materials Science & Processing* 92, no. 3 (2008): 557–563.
9. S. H. Song, K. Nagaich, E. S. Aydil, R. Feist, R. Haley, and S. A. Campbell, “Structure Optimization for a High Efficiency CIGS Solar Cell,” Conference Record of the IEEE Photovoltaic Specialists Conference (2010), 2488–2492.
10. C. Spindler, F. Babbe, M. H. Wolter, et al., “Electronic Defects in Cu(In,Ga)Se₂: Towards a Comprehensive Model,” *Physical Review Materials* 3, no. 9 (2019): 090302.
11. R. Herberholz, V. Nadenau, U. Rühle, C. Köble, H. W. Schock, and B. Dimmler, “Prospects of Wide-Gap Chalcopyrites for Thin Film Photovoltaic Modules,” *Solar Energy Materials and Solar Cells* 49, no. 1–4 (1997): 227–237.
12. Z. Zhang, “Nanoscale Investigation of Potential Distribution in Operating Cu(In,Ga)Se₂ Thin-Film Solar Cells,” (Diss. Karlsruher Institut für Technologie (KIT) 2013).
13. S. H. Wei, S. B. Zhang, and A. Zunger, “Effects of Ga Addition to CuInSe₂ on Its Electronic, Structural, and Defect Properties,” *Applied Physics Letters* 72, no. 24 (1998): 3199–3201.
14. G. Hanna, A. Jasenek, U. Rau, and H. W. Schock, “Influence of the Ga-Content on the Bulk Defect Densities of Cu(In,Ga)Se₂,” *Thin Solid Films* 387, no. 1–2 (2001): 71–73.
15. G. H. Bauer, R. Brüggemann, S. Tardon, S. Vignoli, and R. Kniese, “Quasi-Fermi Level Splitting and Identification of Recombination Losses From Room Temperature Luminescence in Cu (In_{1-x}Ga_x) Se₂ Thin Films Versus Optical Band gap,” *Thin Solid Films* 480–481 (2005): 410–414.
16. R. Gutzler, W. Witte, A. Kanevce, D. Hariskos, and S. Paetel, “ V_{OC} -Losses Across the Band Gap: Insights From a High-Throughput Inline Process for CIGS Solar Cells,” *Progress in Photovoltaics: Research and Applications* 31 (2023): 1023–1031.
17. D. Abou-Ras, T. Kirchartz, and U. Rau, eds., *Advanced Characterization Techniques for Thin Film Solar Cells* (Weinheim, Germany: Wiley, 2016).
18. E. Von Hauff, “Impedance Spectroscopy for Emerging Photovoltaics,” *Journal of Physical Chemistry C* 123, no. 18 (2019): 11329–11346.

19. V. Parvan, A. Mizrak, I. Majumdar, et al., "Cu(In,Ga)Se₂ Surface Treatment With Na and NaF: A Combined Photoelectron Spectroscopy and Surface Photovoltage Study in Ultra-High Vacuum," *Applied Surface Science* 444 (2018): 436–441.
20. D. Abou-Ras, S. Schorr, and H. W. Schock, "Grain-Size Distributions and Grain Boundaries of Chalcopyrite-Type Thin Films," *Journal of Applied Crystallography* 40, no. 5 (2007): 841–848.
21. D. Abou-Ras, R. Caballero, C. A. Kaufmann, et al., "Impact of the Ga Concentration on the Microstructure of CuIn_{1-x}Ga_xSe₂," *Physica Status Solidi Rapid Research Letters* 2, no. 3 (2008): 135–137.
22. B. G. Mendis, L. Bowen, and Q. Z. Jiang, "A Contactless Method for Measuring the Recombination Velocity of an Individual Grain Boundary in Thin-Film Photovoltaics," *Applied Physics Letters* 97 (2010): 092112.
23. B. G. Mendis and L. Bowen, "Cathodoluminescence Measurement of Grain Boundary Recombination Velocity in Vapour Grown p-CdTe," *Journal of Physics: Conference Series* 326, no. 1 (2011): 2–6.
24. M. Krause, A. Nikolaeva, M. Maiberg, et al., "Microscopic Origins of Performance Losses in Highly Efficient Cu(In,Ga)Se₂ Thin-Film Solar Cells," *Nature Communications* 11 (2020): 4189.
25. G. Kakavelakis, A. E. Del Rio Castillo, V. Pellegrini, et al., "Size-Tuning of WSe₂ Flakes for High Efficiency Inverted Organic Solar Cells," *ACS Nano* 11 (2017): 3517–3531.
26. W. K. Metzger, I. L. Repins, M. Romero, et al., "Recombination Kinetics and Stability in Polycrystalline Cu(In,Ga)Se₂ Solar Cells," *Thin Solid Films* 517, no. 7 (2009): 2360–2364.
27. M. Maiberg, T. Hölscher, S. Zahedi-Azad, and R. Scheer, "Theoretical Study of Time-Resolved Luminescence in Semiconductors. III. Trap States in the Band gap," *Journal of Applied Physics* 118 (2015): 105701.
28. M. Maiberg and R. Scheer, "Theoretical Study of Time-Resolved Luminescence in Semiconductors. I. Decay From the Steady State," *Journal of Applied Physics* 116 (2014): 123710.
29. M. Maiberg, F. Bertram, M. Müller, and R. Scheer, "Theoretical Study of Time-Resolved Luminescence in Semiconductors. IV. Lateral Inhomogeneities," *Journal of Applied Physics* 121 (2017): 085703.
30. M. Maiberg, T. Hölscher, E. Jarzembowski, et al., "Verification of Minority Carrier Traps in Cu(In,Ga)Se₂ and Cu₂ZnSnSe₄ by Means of Time-Resolved Photoluminescence," *Thin Solid Films* 633 (2017): 208–212.
31. T. Kirchartz, J. A. Márquez, M. Stolterfoht, and T. Unold, "Photoluminescence-Based Characterization of Halide Perovskites for Photovoltaics," *Advanced Energy Materials* 10, no. 26 (2020): 1904134.
32. J. Bass, "Deviations From Matthiessen's Rule," *Advances in Physics* 21 (1972): 431–604.
33. D. Abou-Ras, A. Nikolaeva, M. Krause, et al., "Optoelectronic Inactivity of Dislocations in Cu(In,Ga)Se₂ Thin Films," *Physica Status Solidi RRL: Rapid Research Letters* 15 (2021): 2100042.
34. J. Li, J. Huang, F. Ma, et al., "Unveiling Microscopic Carrier Loss Mechanisms in 12% Efficient Cu₂ZnSnSe₄ Solar Cells," *Nature Energy* 7, no. 8 (2022): 754–764.
35. A. B. Sproul, "Dimensionless Solution of the Equation Describing the Effect of Surface Recombination on Carrier Decay in Semiconductors," *Journal of Applied Physics* 76, no. 5 (1994): 2851–2854.
36. R. K. Ahrenkiel and J. Dashdorj, "Interface Recombination Velocity Measurement by a Contactless Microwave Technique," *Journal of Vacuum Science and Technology B* 22 (2004): 2063–2067.
37. B. J. Stanbery, D. Abou-Ras, A. Yamada, and L. Mansfield, "CIGS Photovoltaics: Reviewing a New Paradigm," *Journal of Physics D: Applied Physics* 55 (2022): 173001.
38. D. Abou-Ras, A. Nikolaeva, and S. Caicedo Dávila, "No Evidence for Passivation Effects of Na and K at Grain Boundaries in Polycrystalline Cu(In,Ga)Se₂ Thin Films for Solar Cells," *Solar RRL* 3, no. 8 (2019): 1900095.
39. A. Kanevce, J. Moseley, D. Kuciauskas, M. Al-Jassim, and W. K. Metzger, "Quantitative Determination of Grain Boundary Recombination Velocity in CdTe by Combination of Cathodoluminescence Measurements and Numerical Simulations," *IEEE 42nd Photovoltaic Specialist Conference, PVSC* (2015): 1–5, <https://doi.org/10.1109/PVSC.2015.7355654>.
40. J. Quirk, M. Rothmann, W. Li, D. Abou-Ras, and K. P. McKenna, "Grain Boundaries in Polycrystalline Material for Energy Applications: First Principles Modeling and Electron Microscopy," *Applied Physics Reviews* 11 (2024): 011308.
41. J. Brody and A. Rohatgi, "Analytical Approximation of Effective Surface Recombination Velocity of Dielectric-Passivated p-Type Silicon," *Solid State Electronics* 45, no. 9 (2001): 1549–1557.
42. J. Y. W. Seto, "The Electrical Properties of Polycrystalline Silicon Films," *Journal of Applied Physics* 46 (1975): 5247–5254.
43. C. H. Seager, "Grain Boundary Recombination: Theory and Experiment in Silicon," *Journal of Applied Physics* 52 (1981): 3960–3968.
44. S. Thomas, T. Bertram, C. Kaufmann, et al., "Effects of Material Properties of Band-Gap-Graded Cu(In,Ga)Se₂ Thin Films on the Onset of the Quantum Efficiency Spectra of Corresponding Solar Cells," *Progress in Photovoltaics: Research and Applications* 30 (2022): 1238–1246.
45. M. Troviano and K. Taretto, "Urbach Energy in CIGS Extracted From Quantum Efficiency Analysis of High Performance CIGS Solar Cells," *24th European Photovoltaic Solar Energy Conference* (Hamburg, Germany, 2009), 2933–2937.
46. L. Gütay, D. Regesch, J. K. Larsen, et al., "Feedback Mechanism for the Stability of the Band Gap of CuInSe₂," *Physical Review B: Condensed Matter and Materials Physics* 86, no. 4 (2012): 045216.
47. J. M. Merino, J. L. Martín De Vidales, S. Mahanty, R. Díaz, F. Rueda, and M. León, "Composition Effects on the Crystal Structure of Cu-InSe₂," *Journal of Applied Physics* 80, no. 10 (1996): 5610–5616.
48. U. Rau, B. Blank, T. C. M. Müller, and T. Kirchartz, "Efficiency Potential of Photovoltaic Materials and Devices Unveiled by Detailed-Balance Analysis," *Physical Review Applied* 7 (2017): 044016.
49. D. Abou-Ras, "Microscopic Origins of Radiative Performance Losses in Thin-Film Solar Cells at the Example of (Ag,Cu)(In,Ga)Se₂ Devices," *Journal of Vacuum Science and Technology A* 42 (2024): 022803.
50. U. Rau and J. H. Werner, "Radiative Efficiency Limits of Solar Cells With Lateral Band-Gap Fluctuations," *Applied Physics Letters* 84, no. 19 (2004): 3735–3737.
51. C. Stephan, "Structural Trends in Off Stoichiometric Chalcopyrite Type Compound Semiconductors" (Dissertation, Free University Berlin, 2011).
52. O. Cojocaru-Miréidin, M. Raghuvanshi, R. Wuerz, and S. Sadewasser, "Grain Boundaries in Cu(In,Ga)Se₂: A Review of Composition–Electronic Property Relationships by Atom Probe Tomography and Correlative Microscopy," *Advanced Functional Materials* 31 (2021): 2103119.

Supporting Information

Additional supporting information can be found online in the Supporting Information section.